OXFORD UNIVERSITY PRESS Toxicological Sciences

Differential Mouse Pulmonary Dose- and Time Course-Responses to Titanium Dioxide Nanospheres and Nanobelts

Journal:	*Toxicological Sciences*
Manuscript ID:	TOXSCI-12-0207.R1
Manuscript Type:	Research Article
Date Submitted by the Author:	23-Jul-2012
Complete List of Authors:	Porter, Dale; NIOSH, HELD/PPRB; West Virginia University, Department of Physiology and Pharmacology Wu, Nianqiang; West Virginia University, Department of Mechanical & Aerospace Engineering Hubbs, Ann; NIOSH, HELD/PPRB Mercer, Robert; NIOSH, HELD/PPRB; West Virginia University, Department of Physiology and Pharmacology Funk, Kathleen; Experimental Pathology Laboratories, Inc, Meng, Fanke; West Virginia University, Department of Mechanical & Aerospace Engineering Li, Jiangtian; West Virginia University, Department of Mechanical & Aerospace Engineering Wolfarth, Michael; NIOSH, HELD/PPRB Battelli, Lori; NIOSH, HELD/PPRB Friend, Sherri; NIOSH, HELD/PPRB Andrew, Michael; NIOSH, HELD/BEB Hamilton, Raymond; University Of Montana, Center for Environmental Health Sciences SRIRAM, KRISHNAN; CDC-NIOSH, Yang, Feng; West Virginia University, Department of Industrial and Management Systems Engineering Castranova, Vincent; NIOSH, HELD/PPRB Holian, Andrij; University Of Montana, Center for Environmental Health Sciences
Key Words:	nanoparticles < Agents, lung; pulmonary or respiratory system < Respiratory Toxicology, nanoparticles < Respiratory Toxicology
Society of Toxicology Specialty Section Subject Area:	Nanotoxicology [121]

Differential Mouse Pulmonary Dose- and Time Course-Responses to Titanium Dioxide Nanospheres and Nanobelts

Dale W. Porter,[*†] Nianqiang Wu,[‡] Ann F. Hubbs,[*] Robert R. Mercer,[*†] Kathleen Funk,[§] Fanke Meng,[‡] Jiangtian Li,[‡] Michael G. Wolfarth,[*] Lori Battelli,[*] Sherri Friend,[*] Michael Andrew,[*] Raymond Hamilton Jr.,[¶] Krishnan Sriram,[*] Feng Yang,[‖] Vincent Castranova[*] and Andrij Holian[¶]

[*]National Institute for Occupational Safety and Health, Morgantown, WV 26505 USA

[†]West Virginia University, Department of Physiology and Pharmacology, Morgantown, WV 26506 USA

[‡]West Virginia University, Department of Mechanical & Aerospace Engineering, Morgantown, WV 26506 USA

[§]Experimental Pathology Laboratories, Inc., P.O. Box 169, Sterling, VA 20167 USA

[¶]Center for Environmental Health Sciences, University of Montana, Missoula, MT 59812 USA

[‖]West Virginia University, Department of Industrial and Management Systems Engineering, Morgantown, WV 26506, USA

Running Title: Pulmonary Responses to TiO_2 Nanoparticles

Address correspondence to:

Dale W. Porter, Ph.D., Pathology and Physiology Research Branch, Health Effects Laboratory Division, National Institute for Occupational Safety and Health, 1095 Willowdale Road, M/S 2015, Morgantown, WV, 26505, USA. Phone: 304-285-6320 FAX: 304-285-6389 E-mail: DPorter@cdc.gov

DISCLAIMER: The findings and conclusions in this report are those of the authors and do not necessarily represent the views of the National Institute for Occupational Safety and Health.

ABSTRACT

Three anatase titanium dioxide (TiO_2) nanoparticles were prepared; nanospheres (NS), short nanobelts (NB1) and long nanobelts (NB2). These nanoparticles were used to investigate the effect of nanoparticle shape and length on lung toxicity. Mice were exposed (0-30 μg per mouse) by pharyngeal aspiration and pulmonary toxicity was assessed over a 112 day time course. Whole lung lavage data indicated that NB1- and NB2-exposed mice, but not NS-exposed mice, had significant dose- and time-dependent pulmonary inflammation and damage. Histopathological analyses at 112 days post-exposure determined no interstitial fibrosis in any NS-exposed mice, an increased incidence in 30 μg NB1-exposed mice, and significant interstitial fibrosis in 30 μg NB2-exposed mice. At 112 days post-exposure, lung burden of NS was decreased by 96.4% and NB2 by 80.5% from initial deposition levels. At 112 days post-exposure, enhanced dark field microscopy determined that alveolar macrophages were the dominant deposition site, but a fraction of NB1 and NB2 was observed in the alveolar interstitial spaces. For the 30 μg exposure groups at 112 days post-exposure, confocal microscopy and immunofluorescent staining demonstrated that retained NB2 but not NS were present in the interstitium subjacent to the terminal bronchiole near the normal location of the smallest lymphatic capillaries in the lung. These lymphatic capillaries play a critical role in particle clearance, and the accumulation of NB2, but not NS, suggests possible impaired lymphatic clearance by the high aspect ratio particles. In summary, our data indicate that TiO_2 nanoparticle shape alters pulmonary responses, with severity of responses being ranked as NS<NB1<NB2.

INTRODUCTION

In regards to size, particles ranging from 0.1 – 2.5 μm are considered fine, whereas particles with at least one dimension that is 100 nm or less are defined as nanoparticles (Wang *et al.*, 2008). Nanomaterials show size-dependent properties that are different from those of bulk materials (Duan et al., 2001; Tan et al., 2003). Examples are TiO_2 nanomaterials that have been extensively used in various commercial products. TiO_2 nanoparticles (NPs) are used in sunscreen and cosmetics as an ultraviolet (UV) absorber that allows an optically transparent film to be applied to human skin (Hayashi and Kobyashi, 1996). TiO_2 NPs are also employed as photocatalysts to eliminate pollutants in air, drinking water and wastewater systems (Tafen *et al.*, 2009; Wu *et al.*, 2010). TiO_2 nanospheres and nanowires (or nanotubes) are used in dye-sensitized solar cells (DSSCs) (Li *et al.*, 2006; Mor *et al.*, 2006) and biosensors (Yang *et al.*, 2008). Recent studies have revealed that the performance of TiO_2 NPs strongly depends on the particle shape. For example, single-crystalline anatase TiO_2 nanobelts with two dominant surfaces of (101) facets exhibit enhanced photocatalytic activity and higher affinity to oxygen than their nanosphere counterparts with an identical crystal phase and similar specific surface area (Wu *et al.*, 2010). The TiO_2 nanowires in the DSSCs have superior performance over their nanosphere counterparts because the nanowire morphology provides direct conduction paths for the electrons from the point of injection to the collection electrode while maintaining high surface area for dye adsorption (Adachi *et al.*, 2004; Baxter and Aydil, 2005). A recent report has further shown TiO_2 nanobelts exhibit better charge transfer performance than nanosphere counterparts (Wang *et al.*, 2010).

Owing to the unique physical and chemical characteristics, engineered nanomaterials may have distinctive biological effects that are different from their bulk counterparts (Holsapple *et al.*, 2005; Oberdorster *et al.*, 2005; Nel *et al.*, 2006). The increasing manufacture and use of nanomaterials has led to concerns regarding both environmental and human exposures to nanoparticles (Colvin, 2003; Dreher, 2004; Maynard and Kuempel, 2005). In order to predict and reduce the risk of potential human health effects associated with manufactured nanomaterials, it is necessary to study their potential toxicological effects. A few epidemiologic studies have been conducted to examine carcinogenicity of fine TiO_2 in humans, and concluded that no clear evidence of elevated morbidity or mortality due to lung cancer exists (Chen and Fayerweather, 1988; Boffetta *et al.*, 2001; Fryzek *et al.*, 2003; Boffetta *et al.*, 2004; Ramanakumar *et al.*, 2008). However, NIOSH has determined that ultrafine TiO_2, which includes nanoscale TiO_2, is a potential occupational carcinogen (National Institute for Occupational Safety and Health, 2011).

To date, limited studies have investigated the effect of TiO_2 particle shape on toxicity. Primary rat alveolar macrophages exposed in vitro to fine-sized particulate and fibrous TiO_2 particles reported that the fibrous TiO_2 induced a concentration-dependent increase in cytotoxicity but fine-sized spherical TiO_2 did not (Watanabe *et al.*, 2002). In another study (Warheit *et al.*, 2006), rats were dosed by intratracheal (IT) instillation with spherical TiO_2 nanoparticles, nanosized TiO_2 rods and nanosized TiO_2 dots (particle size ~ 10 nm). The nanosized TiO_2 rods and TiO_2 dots produced an acute pulmonary inflammation and cell injury.

In the present study, we test the hypothesis that TiO_2 nanoparticles with different shape will exhibit different toxicity profiles *in vivo*. Specifically, we exposed mice to TiO_2 nanoparticles with different shapes (nanosphere versus nanobelt) and nanobelts with different lengths (short versus long). Dose- and time-course responses of pulmonary inflammation and damage were determined in lung lavage, as well as histopathology studies to investigate the development of pulmonary disease.

MATERIALS AND METHODS

Synthesis and characterization of titanium dioxide nanoparticles.

To prepare the NB2 sample, 1.0 g of anatase titanium dioxide powder was added to 75 ml of 10 M sodium hydroxide aqueous solution. The solution was stirred in ultrasonic bath for 10 min, sealed in a 90 ml Teflon-lined autoclave, and then heated at 200°C for 24 h for hydrothermal treatment. A white fluffy powder was obtained and then washed with 0.1 M HCl and deionized water until the pH was less than 7. The white powder sample was heated at 700 °C for 30 min at a ramp rate of 1 °C/min. To obtain short nanobelts (NB1), the hydrothermally treated samples were heated at a ramp rate of 10 °C/min to break the nanobelts by thermal-gradient induced stress. For comparison tests, the TiO_2 nanospheres (NS) were purchased directly from Alfa Aesar. The nanomaterial samples were observed under a JEOL 7600-F field-emission scanning electron microscope (SEM). The crystal structure of the TiO_2 particles was characterized by X-ray diffraction with Cu Kα radiation (XRD, X'Pert Pro PW3040-Pro, Panalytical Inc.).

TiO_2 nanoparticle suspension. Suspensions of TiO_2 nanoparticles were prepared in dispersion medium (DM; Ca^{2+} and Mg^{2+}-free phosphate buffered saline, pH 7.4, supplemented with 5.5 mM D-glucose, 0.6 mg/ml mouse serum albumin, and 0.01 mg/ml 1,2-dipalmitoyl-sn-glycero-3-phosphocholine) as previously described by our laboratory (Porter *et al.*, 2008). Suspensions of NS were sonicated (5W, 15 minutes) while NB1 and NB2 were mechanically stirred for 1 hour.

Measurement of zeta potential of TiO_2 nanoparticle. Suspensions of TiO_2 nanoparticles (50 μg/mL) were prepared in DM as described above. The zeta potential was measured with a Malvern Zetasizer Nano ZS instrument. For these experiments, the electrophoretic mobility was converted into the zeta potential by means of the Schmolukowski relation.

Animals. Male C57BL/6J mice (6 weeks old) were obtained from Jackson Laboratories (Bar Harbor, ME). Mice were housed one per cage in polycarbonate isolator ventilated cages, which were provided HEPA-filtered air, with fluorescent lighting from 0700 to 1900 hours. Autoclaved Alpha-Dri virgin cellulose chips and hardwood Beta-chips were used as bedding. Mice were monitored to be free of endogenous viral pathogens, parasites, mycoplasms, Helicobacter and CAR Bacillus. Mice were maintained on Harlan Teklad Rodent Diet 7913 (Indianapolis, IN), and tap water was provided ad libitum. Animals were allowed to acclimate for at least 5 days before use. All animals used in this study were housed at the National Institute for Occupational Safety and Health (Morgantown, WV) which is an AAALAC-accredited,

specific pathogen-free, environmentally controlled facility. All procedures involving animals were approved by the NIOSH Institutional Animal Care and Use Committee.

Pharyngeal aspiration exposure of mice. Suspensions of TiO_2 nanoparticles were prepared in DM as described above. Mice were anesthetized with isoflurane (Abbott Laboratories, North Chicago, IL), and, when fully anesthetized, the mouse was positioned with its back against a slant board and suspended by the incisor teeth using a rubber band. The mouth was opened, and the tongue gently pulled aside from the oral cavity. A 50 µl aliquot of sample was pipetted at the base of the tongue, and the tongue was restrained until at least 2 deep breaths were completed (but for not longer than 15 seconds). Following release of the tongue, the mouse was gently lifted off the board, placed on its left side, and monitored for recovery from anesthesia. Mice received DM (vehicle control), NS (15 or 30 µg), NB1 (7.5, 15 and 30 µg) or NB2 (1.875, 7.5, 15 and 30 µg).

Whole lung lavage. At 1, 3, 7, 28 and 112 days post-exposure, mice were euthanized with an i.p. injection of sodium pentobarbital (>100 mg/kg body weight) followed by exsanguination. A tracheal cannula was inserted and whole lung lavage (WLL) was performed through the cannula using ice cold Ca^{2+} and Mg^{2+}-free phosphate buffered saline, pH 7.4, supplemented with 5.5 mM D-glucose (PBS). The first lavage (0.6 ml) was kept separate from the rest of the lavage fluid. Subsequent lavages, each with 1 ml of PBS, were performed until a total of 4 ml of lavage fluid was collected. WLL cells were isolated by centrifugation (650 x g, 5 minutes, 4°C). An aliquot of the acellular

supernatant from the first WLL (WLL fluid) was decanted and transferred to tubes for analysis of lactate dehydrogenase (LDH) and albumin. The acellular supernatants from the remaining lavage samples were decanted and discarded. WLL cells isolated from the first and subsequent lavages for the same mouse were pooled after resuspension in PBS, centrifuged a second time (650 x g, 5 min, 4°C), and the supernatant decanted and discarded. The WLL cell pellet was then resuspended in PBS and placed on ice. Total WLL cell counts were obtained using a Coulter Multisizer 3 (Coulter Electronics, Hialeah, FL), and cytospin preparations of the WLL cells were made using a cytocentrifuge (Shandon Elliot Cytocentrifuge, London). The cytospin preparations were stained with modified Wright-Giemsa stain, and cell differentials were determined by light microscopy.

WLL fluid LDH activity and albumin concentration measurements. WLL fluid LDH activities were evaluated as a marker of cytotoxicity. WLL fluid LDH activities were determined by monitoring the LDH catalyzed oxidation of lactate to pyruvate coupled with the reduction of NAD at 340 nm using a commercial assay kit (Roche Diagnostics Systems, Montclair, NJ). WLL fluid albumin concentrations were determined as an indicator of the integrity of the blood–pulmonary epithelial cell barrier. WLL fluid albumin was determined colorimetrically at 628 nm based on albumin binding to bromcresol green, using a commercial assay kit (Sigma Chemical Company, St. Louis, Mo). Both the WLL fluid LDH and albumin assays were conducted using a COBAS MIRA Plus (Roche Diagnostic Systems, Montclair, NJ).

Determination of TiO_2 lung burden. Lung samples were placed in sealed vessels for digestion. The following was added to each vessel: 3 mL of 70% nitric acid, 1 mL of 30% hydrogen peroxide and 0.1 mL of 50% hydrofluoric acid. Either one or two digestion blanks (empty digestion vessels with digestion reagents) were prepared for each digestion set. TiO_2 spiked liver tissue controls were run concurrently with the lung samples. All samples and controls were digested using a Milestone Ethos Plus microwave system at 400W power with a temperature set point of 140°C for 10 minutes, followed by a cycle at 600W with a set point of 180°C for 25 minutes. After cooling, the digests were diluted with ultrapure water to approximately 30 g and transferred into pre-cleaned, pre-weighed polyethylene bottles. The bottles were reweighed to calculate the exact mass of digestate. For DM-exposed mouse lungs, a solution of internal standard Sc (scandium) was then weighed into the digestates. Due to high levels of analyte in the NS and NB2 lung samples, it was necessary to prepare dilutions which were analyzed in a separate analytical runs. The internal standard Sc was also added to the dilutions as a liquid solution. Elemental Ti (^{47}Ti and/or ^{49}Ti) was then quantified using a VG Axiom high-resolution ICP-MS against Ti standards, which also contained the internal standard, from 2 to 100 ppb. The calculation of tissue TiO_2 from Ti determinations was done as follows. First, the mass of Ti determined for a sample was divided by the atomic weight of Ti to obtain the number of moles of Ti in that sample. Next, to calculate the mass of TiO_2, the number of moles of Ti was multiplied by the molecular weight of TiO_2. The basis for the latter calculation is that the number of moles of Ti equals the number of moles of TiO_2.

TiO_2 nanoparticle visualization in the lung. Sections of the fixed left lung were embedded in paraffin. Sections (5 μm thick) were collected on precleaned slides, deparaffinized and briefly stained with 1% Toluidine blue before being coverslipped. Slides were imaged using a high signal-to-noise, dark field-based illumination on an Olympus BX-41 microscope (CytoViva, Auburn, AL) at 100x with oil immersion. Verification of the particles imaged as nanoparticles was based on using the CytoViva Hyperspectral imaging system to capture the spectrum (400-1000nm) and matching the spectra of the particle with the spectra from nanoparticle-doped standard sections. Images were captured with a Dage MTI digital camera (2048x2048, Dage, Michigan City, IN). Additional images of a calibration slide were taken to ensure accuracy of the magnification.

Histopathology. Mice for histopathology were not lavaged. Mice were euthanized by an overdose of pentobarbital (>100 mg/kg body weight, i.p.) followed by transection of the abdominal aorta to provide exsanguination. The lungs were rapidly removed and fixed by intratracheal perfusion with 1 mL of 10% neutral buffered formalin. Lungs were trimmed the same day, processed overnight in a tissue processor, and embedded in paraffin. The lungs were stained with hematoxylin and eosin for routine morphologic assessment, and with Masson's trichrome and Sirius Red for evaluating fibrosis.

Demonstration of pulmonary lymphatics by podoplanin and e-cadherin dual-label immunofluorescence. Pulmonary lymphatics were demonstrated using podoplanin and e-cadherin dual-label immunofluorescence as previously described

(Porter *et al.*, 2010). In brief, the lymphatics were stained using a hamster anti-podoplanin primary antibody (Novus Biologicals, Littleton, CO) and DyLight® conjugated goat anti-hamster (Jackson ImmunoResearch, West Grove, PA) secondary antibody. Pulmonary architecture was demonstrated using a mouse anti-e-cadherin primary antibody with an Alexa-488 labeled donkey anti-mouse (Invitrogen, Carlsbad, CA) secondary. With this technique, lymphatics fluoresce intensely red because of high levels of podoplanin expression (Baluk and McDonald, 2008) without e-cadherin expression, while normal pulmonary architecture is demonstrated by e-cadherin staining in epithelium (green), staining of endogenous mouse IgG by the secondary antibody (green), and/or combined e-cadherin and podoplanin staining (orange). This allows both the lymphatics and their location to be demonstrated in tissue sections. Pulmonary lymphatic photomicroscopy was conducted using a Zeiss LSM 510 upright confocal microscope using fluorescence capabilities to demonstrate the lymphatics with superimposed transmitted light to demonstrate NS and NB.

Statistics. Statistical comparisons between doses for each nanoparticle at a specific post-exposure time were performed separately for each post-exposure time using analysis of variance (ANOVA) with post-hoc t-tests for pair-wise comparison of dose groups. Similar analyses were performed to compare post-exposure time effect for each nanoparticle. Since variance estimates were different across dose groups, the ANOVA models were estimated using an unequal variance model available from SAS PROC MIXED. All statistical tests were two tailed with significance level equal to 0.05.

Since the pathology data consisted of ordinal scores then comparisons between control and TiO_2-exposed mice at each time, comparisons across time for each exposure group were accomplished using two separate one-way nonparametric analyses or variance (ANOVAs). Exact tests were used because of the high number of tied values in the data. The nonparametric ANOVA was performed using SAS Proc NPAR1WAY with exact Kruskal-Wallis tests for multi-group comparisons and exact Wilcoxon tests for post hoc pair-wise comparisons. All statistical tests were two-tailed and performed at the 0.05 significance level.

RESULTS

Physico-Chemical Properties of Titanium Dioxide Nanoparticles

SEM images and the corresponding size distributions for NB1 (Figure 1), NB2 (Figure 2) and NS (Figure 3) were determined. Both NB1 and NB2 exhibited nanobelt morphology. A majority of NB1 were 1-5 μm long, with widths between 40-120 nm (Figure 1). Most of the NB2 had lengths from 6-12 μm, and widths between 60-140 nm (Figure 2). The median aspect ratio was around 30 and 80 for NB1 and NB2, respectively. Dry NS had a diameter of 70-190 nm (Figure 3), while the hydrodynamic size of NS in DM was determined to be 354.2 nm. All three types of TiO_2 nanoparticles exhibited the anatase phase as shown in the XRD pattern (Figure 4). The zeta potentials of the TiO_2 nanoparticles in the DM used for the in vivo experiments were -12.4 mV (NS), -12.5 mV (NB1), and -9.35 mV (NB2), respectively.

Whole Lung Lavage (WLL) Studies

Acute pulmonary inflammation dose-responses after exposure to TiO_2 nanoparticles were assessed by quantitating WLL polymorphonuclear leukocytes (PMNs) at 1, 3 and 7 days post-exposure. Exposure of mice to NS did not cause a significant increase in WLL PMNs versus vehicle control (Figure 5, panel A). In contrast, mice exposed to NB1 (Figure 5, panel B) and NB2 (Figure 5, panel C) both exhibited dose-dependent increases in WLL PMNs versus vehicle-exposed mice. For 30 μg NB1 dose, a non-statistically significant ($p>0.05$) decrease in WLL PMNs was observed at 3 days post-exposure in comparison to 1 or 7 days post-exposure (Figure 5, panel B).

The integrity of the lung blood-gas barrier was assessed by measuring first WLL albumin concentrations. Mice exposed to NS did not have a statistically significant increase in albumin concentrations versus vehicle control (Figure 6, panel A). NB1-exposed mice had elevated concentrations of albumin in the first WLL fluid at all three post-exposure times examined (Figure 6, panel B). Likewise, mice exposed to NB2 also had elevated concentrations of albumin in the first WLL fluid at all three post-exposure times (Figure 6, panel C).

Cytotoxicity in the lung after exposure to TiO_2 nanoparticles was assessed from LDH activity in the first WLL after 1, 3 and 7 days post-exposure. Mice exposed to NS did not have increased LDH activities versus vehicle control (Figure 7, panel A). However, mice exposed to 15 and 30 μg NB1 did have significantly increased LDH activities in comparison to DM-exposed controls at 1 and 3 days post-exposure, but by 7 days post-exposure only the 30 μg NB1-exposed mice were still elevated versus controls (Figure 7, panel B). Mice exposed to 7.5-30 μg NB2 had significantly higher LDH activities versus DM controls at all three post-exposure times (Figure 7, panel C).

To determine the time-course of pulmonary responses to each nanomaterial, mice were exposed to either DM (vehicle control) or 30 μg of NS, NB1 or NB2 and markers of pulmonary inflammation and damage were assessed from 1-112 days post-exposure. In terms of pulmonary inflammation as determined by WLL PMNs, both NB1 and NB2 were significantly higher than DM (vehicle-control) and NS at 1, 3 and 7 days post-exposure (Figure 8, panel A). However, by 28 days post-exposure, WLL PMNs in all nanoparticle-exposed mice were back to control levels. Similarly, first WLL fluid albumin concentrations (Figure 8, panel B) and first WLL fluid LDH activities (Figure 8, panel C) for mice exposed to NB1 and NB2 were significantly higher than DM (vehicle-control) and NS at 1, 3 and 7 days post-exposure, but at 28 and 112 days post-exposure first WLL fluid albumin concentrations and LDH activities for all nanoparticle-exposed mice were back to control levels.

TiO_2 Lung Burden and Clearance

Based on the acute time course data, which indicated pulmonary inflammation and damage induced by NS was minimal and damage induced by NB2 was the greatest of the three nanoparticles tested, lung burden and clearance of these two nanoparticles was determined over the 112 day time course (Figure 9). Initial deposition of NS and NB2 showed similar lung burdens. By 28 days post-exposure, lung burden of NS was decreased 69.0% and NB2 by 54.9% from lung burden levels at 1 hour post-exposure. There was no statistical difference between lung burden of NS and NB2 at 28 days post-exposure. By 112 day post-exposure lung burden of NS was decreased 96.4% and NB2 by 80.5% from lung burden levels at 1 hour post-exposure. In contrast to 28 days

post-exposure, NS lung burden was significantly lower than that for NB2 exposed mice at 112 days post-exposure.

Imaging Studies

As shown in the representative FESEM micrographs (Figure 10) obtained at 112 days post-exposure, large concentrations of nanoparticles were observed in the interior of the alveolar macrophages (AMs) for both types of nanobelts (NB1 and NB2) as well as in the nanosphere-treated lungs (NS).

Enhanced dark field microscopy examination of mice exposed to DM, NS (30 μg), NB1 (30 μg) or NB2 (30 μg) at 112 days post-exposure showed that AMs were the dominant deposition site for all three types of TiO_2 nanoparticles in this study (Figure 11). Nanospheres outside of AMs were rarely observed as essentially all NS were cleared by AM. However, a fraction of the NB1 and NB2 were observed in the alveolar interstitial spaces.

Histopathology

Histopathology scores for alveolitis, histiocytic alveolitis, phagocytosed nanoparticles and interstitial fibrosis are presented in Table 1. Phagocytosed TiO_2 nanoparticles in AMs were significantly higher for mice exposed to NS (7.5 and 30 μg) and NB1 (30 μg) at both 28 and 112 days post-exposure compared to vehicle-exposed controls. There was also a tendency for the nanobelts to cluster or aggregate within cell cytoplasm of AMs compared to the nanospheres. The nanospheres tended to be slightly

more dispersed within the cytoplasm of AMs that had phagocytosed the administered material (Supplemental Figure 1).

Histopathological examination of the tracheobronchial lymph nodes also showed phagocytosed NB1 and NB2 at the 30 μg dose more frequently than NS at 28 days post-exposure with persistence of phagocytosed nanoparticles at 112 days post-exposure. Phagocytosis of NS (30 μg dose) was also more evident in tracheobronchial lymph nodes at 112 days post-exposure compared to 28 days post-exposure.

Alveolitis had the highest incidence and composite score for the 30 μg NB2-exposed mice at 28 days post-exposure compared to other affected groups. At 112 days post-exposure, alveolitis was uniformly minimal and fewer of the treated groups had alveolitis.

Interstitial fibrosis was only observed in mice exposed to 30 μg NB1 and NB2 at 28 days post-exposure, although neither was significantly higher in comparison to DM-exposed vehicles controls. At 112 days post-exposure, interstitial fibrosis persisted at an increased incidence for 30 μg NB1-exposed mice, but was still not significantly increased versus DM-exposed mice. In addition, the 7.5 μg NB1 group had a single incidence of interstitial fibrosis. In contrast, mice exposed to 30 μg NB2 at 112 days post-exposure had interstitial fibrosis which was significantly increased versus DM-exposed controls.

A detailed histopathologic evaluation for infiltrates in the interstitium subjacent to the epithelium at the bronchioloalveolar junction in the 30 μg dose at the 112 day post-exposure time point was conducted to evaluate cellular infiltrates corresponding to particle accumulation near bronchiolar lymphatics (see below). Histiocytic inflammation

subjacent to the epithelium of the terminal bronchioles was not observed in nanosphere-exposed mice (Figure 12, panel A) but subtle histiocytic inflammation was observed in 3 of 6 mice exposed to NB1 (Figure 12, panel B) and 4 of 6 mice exposed to NB2 (Figure 12, panel C).

Confocal dual-label immunofluorescence

Confocal dual label immunofluorescence for e-cadherin and podoplanin in mice at 112 days post-exposure to the highest dose, revealed important differences between NS and NB in sites of particle accumulation and suggested a role for the peribronchiolar lymphatic capillaries in this altered deposition. In NS-exposed mice, normal lymphatics were demonstrated in perivascular and periobronchiolar locations without evidence of NS accumulation (Figure 13, panels A & B). In the six NB1-exposed mice, peribronchiolar lymphatics were unusually prominent in two mice (Figure 13, panel C) and in two other mice NBs could be demonstrated in the perivascular and peribronchiolar interstitium (Figure 13, panel D), a common site for pulmonary lymphatics. In NB2-exposed mice, NB aggregates at the bronchioloalveolar junction were observed in all six mice (Figure 13, panel E). Dilated peribroncholar lymphatics were observed in two NB2-exposed mice (Figure 13, panel E) and NB could be demonstrated within the endothelium of the dilated lymphatics in these mice (Figure 13, panel F). No changes were observed in the subpleural lymphatics in any exposure group.

DISCUSSION

The overall hypothesis of this study was that nanoparticles with different shapes will exhibit different pulmonary toxicity profiles in vivo. To test this hypothesis, TiO_2 nanoparticles with the same crystalline structure (anatase), but with different shapes, i.e. nanospheres (spherical) and nanobelts (fiber-like), were prepared. The nanobelts also had different lengths, with NB1 being shorter than NB2. Thus, in addition to examining the effect of nanoparticle shape we also were able to test the effect of nanobelt length on lung toxicity.

Pulmonary inflammation was assessed by quantitating WLL PMNs and histopathologically by assessing alveolitis. Exposure of mice to NS, at lung burdens of 30 μg or less, caused no pulmonary inflammation at any post-exposure time as assessed by either endpoint. This finding is similar to previous studies in both mice and rats using various exposure techniques. Mice exposed by whole body inhalation to anatase TiO_2 (25 nm) reported no pulmonary inflammation (Rossi *et al.*, 2010). In another study, rats which received nanoscale TiO_2 dots by intratracheal (IT) instillation only had transient pulmonary inflammation and cell injury at one day post-exposure (Warheit *et al.*, 2006) whereas another rat IT study (Cho *et al.*, 2010) reported no pulmonary inflammation 24 hours post-exposure to TiO_2 nanospheres (30-40 nm).

In contrast to NS, mice exposed to NB1 and NB2 had dose-dependent pulmonary inflammation as measured by WLL PMNs, with increases induced by NB1 being less than NB2. For both NB1- and NB2-exposed mice, WLL PMNs returned to vehicle-exposed control levels by 28 days post-exposure. Alveolitis tended to be minimal and focal albeit with a greater incidence and distribution in mice exposed to NB2 than NB1 at 30 μg dose level, suggesting not only the length of these nanoparticles

but the dosage played a role in the development of pulmonary inflammation, an observation consistent with the WLL PMN data.

To date, limited studies have investigated the effect of TiO_2 particle shape on toxicity. Primary rat AMs exposed in vitro to fine-sized particulate and fibrous TiO_2 particles reported that the fibrous TiO_2 (1-2 μm long) induced a concentration-dependent increase in LDH release, whereas particulate spherical TiO_2 (particle size=1.8 μm) did not (Watanabe *et al.*, 2002). In an in vivo study of TiO_2 nanoparticles (Warheit *et al.*, 2006), rats received nanoscale TiO_2 rods (particle size, 200 nm x 35 nm) or nanoscale TiO_2 dots (particle size ~ 10 nm) by intratracheal (IT) instillation. The nanoscale TiO_2 rods and TiO_2 dots only produced transient pulmonary inflammatory and cell injury effects at 24 hours post-exposure. In the present study, in contrast to TiO_2 NS, mice exposed to NB1 and NB2 had dose-dependent pulmonary inflammation and damage, with increases induced by NB1 being less than NB2. For both NB1- and NB2-exposed mice, pulmonary inflammation and damage returned to vehicle-exposed control levels by 28 days post-exposure. Because fiber length is a major determinant of toxicity (Donaldson *et al.*, 2006), and the length of the nanorods studied by Warheit et al (2006) was very small (200 nm) compared to NB1 and NB2 in our study, it is not surprising that NB1 and NB2 induced greater pulmonary inflammation and damage.

Enhanced dark field microscopy determined that AMs were the dominant location for all three types of nanoparticles at 112 days post-exposure. In the case of the spherical nanoparticles, NS outside of AMs were rarely observed as essentially all nanospheres were cleared by AMs. For NB-1 and NB2-exposed mice, a small fraction of the nanobelts were also observed in the alveolar interstitial spaces This suggests that

AMs were more efficient at phagocytosis and clearance of the NS particles than the nanobelt particles. This hypothesis is supported by histopathological findings that NS- and NB1-exposed mice had higher levels of phagocytosed nanoparticles in relation to NB2 exposed mice, and lung burden data which showed greater clearance of NS than NB2 nanoparticles from the lung at 112 days post-exposure.

The lymphatics are a major route for particle clearance from the lung to the lung-associated lymph nodes (Lauweryns and Baert, 1974; Harmsen *et al.*, 1985; Harmsen *et al.*, 1987; Takahashi and Patrick, 1987). For spherical particles, transport in the lymphatics is within phagocytic cells (Harmsen *et al.*, 1985; Harmsen *et al.*, 1987). Migration of phagocytic cells into the lymphatics is controlled at the level of small lymphatic capillaries which have no basement membrane and are lined by a loose endothelium which plays a critical role in transmigration of phagocytic cells (Pepper and Skobe, 2003; Johnson and Jackson, 2008). In our study, we were able to use podoplanin staining in conjunction with e-cadherin to visualize the lymphatics of the deep lung (Baluk and McDonald, 2008; Kambouchner and Bernaudin, 2009; Porter *et al.*, 2010). The smallest lymphatic capillaries were seen in the interstitium adjacent to the terminal bronchioles near the bronchioloalveolar junction. We saw an accumulation of nanobelts, but not NS, in the interstitium of the bronchioloalveolar junction and dilated lymphatics containing intra-endothelial nanobelts were occasionally observed. This suggests that macrophages containing nanobelts migrated to the site of lymphatic capillaries but lymphatic clearance may have been altered, suggesting the lymphatics as a potential site for the impaired clearance seen in the NB2-exposed mice.

Interestingly, in workers exposed to asbestos, a durable high aspect ratio particle, early changes in the deep lung occur within the wall of the smallest airways of the human lung, the respiratory bronchioles and the adjacent alveolar ducts (Craighead *et al.*, 1982; Wright and Churg, 1984; Roggli *et al.*, 2010), which are also the location of small lymphatic capillaries (Leak, 1980). In addition, the formation of new lymphatics, lymphangiogenesis, is associated with chronic obstructive pulmonary disease and severity of airway obstruction in man (Hardavella *et al.*, 2011). In addition, abnormal lymphangiogenesis extending into the alveolar region of the lung is associated with idiopathic pulmonary fibrosis in man (El-Chemaly *et al.*, 2009). We have previously described dilation of peribronchiolar and subpleural lymphatics in mice aspirating multi-walled carbon nanotubes (Porter *et al.*, 2010). Importantly, inflammation can cause lymphangiogenesis (Baluk *et al.*, 2005; El-Chemaly *et al.*, 2008). Therefore, additional studies will be needed to determine whether 1) the increased prominence and dilation of pulmonary lymphatics is a response to inflammation associated with impaired clearance of high aspect ratio particles, or 2) the lymphatic changes contribute to the impaired clearance of high aspect ratio particles, such as NB2 and multi-walled carbon nanotubes.

Within the AM itself, incorporation of nanobelts was complete with relatively few nanobelts found to be protruding outside the cell body, as determined by FESEM. The generally complete incorporation is significantly different from other nanoparticles of similar dimensions. For instance, multi-walled carbon nanotubes are frequently observed to partially penetrate AMs as well as other cell membranes such as the alveolar epithelium of the lungs (Porter *et al.*, 2010).

Data obtained in this study suggest that the differential inflammatory responses to the TiO_2 nanoparticles in this study are dependent on clearance of the nanoparticles. Assessment of WLL PMNs showed that mice exposed to NS did not cause significant inflammation, but mice exposed to NB1 and NB2 did. By 28 days post-exposure, WLL PMNs in all nanoparticle-exposed mice were back to control levels. However, alveolitis for the 30 μg NB2 exposed mice at 28 days post-exposure remained significantly elevated compared to vehicle-exposed controls. At 112 days post-exposure, WLL PMNs for all exposure groups were back to control levels and alveolitis was uniformly minimal and fewer of the treated groups had alveolitis. These observations are consistent with clearance of the nanoparticles from the lung, which showed lung burden of NS decreased by 69.0% at 28 days post-exposure and by 96.4% at 112 days post-exposure. For NB2, lung burden was decreased by 54.9% at 28 days post-exposure, and at 112 day post-exposure by 80.5%.

Furthermore, several lines of evidence also suggest that the differential fibrotic responses to the TiO_2 nanoparticles in this study are dependent on differential clearance of the nanoparticles, which in turn is related to shape differences. The lung burden of NS was significantly lower than NB2 at 112 days post-exposure, indicating that NS were cleared better from the lung. This is consistent with the observations made using enhanced dark field microscopy, which showed that AMs contained NS and nanoparticles were rarely observed outside the AMs whereas NB2 were observed in both AMs and in the alveolar interstitial spaces. The basis for the difference in clearance of NS and NB2 is likely due to difference in shape, i.e. sphere versus fiber-like morphology. The length of the NB2 nanoparticles (6-12 μm) is equal to or greater than

diameter of the mouse AM, which has been reported to be 7.23 ± 0.55 μm (Stone *et al.*, 1992). This may have led to some of the NB2 escaping AM-mediated phagocytosis, allowing them to enter the alveolar interstitial spaces, and these NB2 nanoparticles are likely responsible for the decreased lung clearance. Since NB2 exposure, but not NS, significantly increased pulmonary fibrosis at 112 days post-exposure, it seems reasonable that it is possible that the fraction of NB2 that escaped AM-mediated phagocytosis and entered the alveolar interstitial space contributes to the development of fibrosis.

A previously published study from our research group compared the in vitro responses of mouse primary AMs to the same three TiO_2 nanoparticles examined in this study (Hamilton *et al.*, 2009). One of the major findings of that study was that primary AMs exhibit differential responses to TiO_2 nanoparticles based on differences in their shape. In addition, the ranking of these nanomaterials was NS<NB1<NB2. Thus, the overall conclusion regarding the in vitro toxicity of these TiO_2 nanomaterials is entirely consistent with the in vivo study results reported here. In addition, we reported that NB2 activated the NLRP3 inflammasome in vitro, whereas NS and NB1 did not. We are currently investigating if NS and NB2 exhibit a similar differential activation of the NLRP3 inflammasome in vivo. Since inflammasome activation is known to occur in response to other well-known human health hazards, such as silica and asbestos, investigating the possible differential activation of the NLRP3 inflammasome by NS and NB2 may offer additional insights into the mechanisms participating in the development of fibrosis.

In summary, our data indicate that TiO_2 nanoparticle shape and length affect pulmonary responses. In terms of pulmonary inflammation and damage caused by exposure to the three TiO_2 nanoparticles tested in this study, the potency is NS<NB1<NB2. Of the three TiO_2 nanoparticles tested, only the nanobelts caused development of pulmonary fibrosis, which correlated with the severity of pulmonary inflammation. The archetype paradigm to predict fiber toxicity suggests that fibers that have a diameter <3 μm, length >15 μm, and are biopersistant should be considered as potentially pathogenic. Recently it has been determined that these same physiochemical properties may also predict pathogenicity of fiber-like nanomaterials, based on studies which have reported length dependent toxicity of MWCNT (Poland *et al.*, 2008; Murphy *et al.*, 2011) and nickel nanowires (Poland *et al.*, 2011). Data from the present study determined pulmonary toxicity and pathogenesis is related to TiO_2 nanoparticle shape and length, thus adding to the evidence that the archetype paradigm to predict fiber toxicity also applies to fiber-like nanomaterials.

Figure 1. Characterization of nanobelt sample NB1. Panel A. Low-magnification SEM image of nanobelt sample NB1. Panel B. High-magnification SEM image of nanobelt sample NB1. Panel C. Histogram of lengths of nanobelt sample NB1. Panel C. Histogram of widths of nanobelt sample NB1.

Figure 2. Characterization of nanobelt sample NB2. Panel A. Low-magnification SEM image of nanobelt sample NB2. Panel B. High-magnification SEM image of nanobelt sample NB2. Panel C. Histogram of lengths for nanobelt sample NB2. Panel D. Histogram of widths for nanobelt sample NB2.

Figure 3. Characterization of nanosphere sample NS. Panel A. SEM image of nanosphere sample NS. Panel B. Size distribution for nanosphere sample NS.

Figure 4. XRD patterns for nanospheres (NS), short (NB1) and long (NB2) nanobelt samples.

Figure 5. Acute pulmonary inflammation dose-responses after exposure to TiO_2 nanoparticles. WLL PMNs were determined at 1, 3 and 7 days post-exposure as an indicator of pulmonary inflammation. Panel A. WLL PMNs determined after exposure to NS. Panel B. WLL PMNs determined after exposure to NB1. Panel C. WLL PMNs determined after exposure to NB2. Values represent means ± SE (n=6-8). For a given post-exposure time, bars with different letters are significantly different from each other ($p<0.05$).

Figure 6. Acute pulmonary first WLL fluid albumin dose-responses after exposure to TiO_2 nanoparticles. First WLL fluid albumin concentrations were determined at 1, 3 and 7 days post-exposure as an indicator of the integrity of the lung blood-gas barrier. Panel A. First WLL fluid albumin concentrations determined after exposure to NS.. Panel B. First WLL fluid albumin concentrations determined after exposure to NB1. Panel C. First WLL fluid albumin concentrations determined after exposure to NB2. Values represent means ± SE (n=6-8). For a given post-exposure time, bars with different letters are significantly different from each other ($p<0.05$). Bars with two letters indicate differences exist between this bar and both lower and/or higher doses at the same post-exposure time.

Figure 7. Acute pulmonary first WLL fluid LDH dose-responses after exposure to TiO_2 nanoparticles. First WLL fluid LDH was determined at 1, 3 and 7 days post-exposure as an indicator of the cytotoxicity. Panel A. First WLL fluid LDH activities determined after exposure to NS. Panel B. First WLL fluid LDH activities determined after exposure to NB1. Panel C. First WLL fluid LDH activities determined after exposure to NB2. Values represent means ± SE (n=6-8). For a given post-exposure time, bars with different letters are significantly different ($p<0.05$). Bars with two letters indicate differences exist between this bar and both lower and/or higher doses at the same post-exposure time.

Figure 8. Time course of pulmonary inflammation and damage after exposure to TiO_2 nanoparticles. Panel A. WLL PMNs were determined as an indicator of pulmonary

inflammation. Panel B. First WLL fluid albumin concentrations were determined as an indicator of the integrity of the lung blood-gas barrier. Panel C. First WLL fluid LDH was determined as an indicator of nanoparticle-induced cytotoxicity. Values represent means ± SE (n=6-8). For a given post-exposure time, bars with different letters are significantly different from each other ($p<0.05$).

Figure 9. TiO_2 nanoparticle lung burden. The lung burden of TiO_2 NS and NB2 were determined from 1 hour to 112 days post-exposure. Values represent means ± SE (n=5). For a given post-exposure time, bars with different letters are significantly different ($p<0.05$).

Figure 10. Field emission scanning electron microscope (FESEM) showing interior view of AMs isolated from mice exposed to DM, NS (30 μg), NB1 (30 μg) or NB2 (30 μg) at 112 days post-exposure. Arrows indicate nanoparticles within AMs.

Figure 11. Enhanced dark field microscopy examination of mice exposed to DM, NS (30 μg), NB1 (30 μg) or NB2 (30 μg) at 112 days post-exposure. Nanospheres and nanobelts are generally white against the dull colored background of tissue in these images. Arrows in the figure indicate alveolar macrophages which contain NS, NB1 or NB2 in the respective figures. Filled triangles indicate nanobelts which are either contained in or penetrating into the alveolar interstitial space. NS were infrequently observed in the lungs as the total lung burden remaining at 112 days post-exposure

was less than 4% of initial lung burden. No nanoparticles were observed in lungs from DM-exposed mice.

Figure 12. Bronchioloalveolar junction at 112 days post-exposure to 30 µg TiO2 nanoparticles. Panel A. Normal bronchioloalveolar junction in a NS-exposed mouse. Panel B. Rare NB1 (arrows) and small numbers of infiltrating histiocytes (*) in a NB1-exposed mouse. Panel C. Rare NB2 (arrows) and small numbers of infiltrating histiocytes (*) in a NB1-exposed mouse. Reference bar is 10 microns.

Figure 13. Podoplanin/e-cadherin dual-label immunofluorescence at 112 days post-exposure to 30 µg of a TiO2 nanoparticle. Podoplanin (red) is expressed in lymphatic endothelium and alveolar type I cells. E-cadherin (green) is expressed in the intercellular junction of airway epithelial cells and lightly stains alveolar type I cells. In the combined images, the lymphatic endothelium is bright red, alveolar type I cells are orange, intercellular junctions of airway epithelial cells are bright green and the vascular endothelium is pale green. Panel A. In a mouse exposed to NS, peribronchiolar lymphatics (solid arrow) are small structures subjacent to the bronchiolar epithelium (dashed arrows) and are easily distinguished from the vasculature (V). Panel B. In a mouse exposed to NS, perivascular lymphatics (solid arrows) are in the tunica adventitia of large vessels (V). Panel C. In a mouse exposed to NB1, the smallest lymphatic capillaries are located near the bronchioloalveolar junction (solid arrow), the peribronchiolar lymphatics are unusually prominent and occasionally dilated (L) but easily distinguished from the vasculature (V). A macrophage (dashed) arrow is being

cleared by mucociliary clearance. Panel D. In a mouse exposed to NB1, transmitted light is being used to visualize aggregates of NB1 nanobelts in sites where the lymphatics are frequently located: NB1 (solid arrow) are in the tunica adventitia of a large vessel (V) and in the peribronchiolar interstitium (dashed arrow). Panel E. In a mouse exposed to NB2, transmitted light is being used to visualize aggregates of NB2 nanobelts (solid arrows) in the interstitium subjacent to the epithelium at the bronchioloalveolar junction. A peribronchiolar lymphatic (L) is markedly dilated and macrophages (dashed arrow) are adhered to the lymphatic endothelium. Panel F. Refocusing and a higher magnification of the section in Panel E reveals a NB2 (solid arrow) in the lymphatic endothelium. Reference bar is 5 microns.

Supplementary Figure 1. Light microscopic images of AMs obtained at 28 days post-exposure. Panel A. AM from a mouse exposed to 30 μg NS showing numerous well dispersed NS. Panel B. AM from a mouse exposed to 30 μg NB1 showing apparent cytoplasmic expansion and somewhat less dispersed particles. Panel C. AM from a mouse exposed to 30 μg NB2 which shows apparent cytoplasmic expansion and particles that are somewhat less dispersed than the NS. Bar=10 μm.

FUNDING

This work was supported by National Science Foundation (CBET-0834233) and (CBET-1065931), and The National Institute of Environmental Health Sciences [1RC2ES018742-01, P20 RR017670 to A. Holian]. The resource and facilities used at West Virginia University were partially supported by National Science Foundation [EPS 1003907].

REFERENCES

Adachi, M., Murata, Y., Takao, J., Jiu, J. T., Sakamoto, M., and Wang, F. M. (2004). Highly efficient dye-sensitized solar cells with a titania thin-film electrode composed of a network structure of single-crystal-like TiO2 nanowires made by the "oriented attachment" mechanism. *J Am Chem Soc* **126**, 14943-14949.

Baluk, P., and McDonald, D. M. (2008). Markers for microscopic imaging of lymphangiogenesis and angiogenesis. *Ann N Y Acad Sci* **1131**, 1-12.

Baluk, P., Tammela, T., Ator, E., Lyubynska, N., Achen, M. G., Hicklin, D. J., Jeltsch, M., Petrova, T. V., Pytowski, B., Stacker, S. A., Yla-Herttuala, S., Jackson, D. G., Alitalo, K., and McDonald, D. M. (2005). Pathogenesis of persistent lymphatic vessel hyperplasia in chronic airway inflammation. *J Clin Invest* **115**, 247-257.

Baxter, J. B., and Aydil, E. S. (2005). Nanowire-based dye-sensitized solar cells. *Appl Phys Lett* **86**.

Boffetta, P., Gaborieau, V., Nadon, L., Parent, M. F., Weiderpass, E., and Siemiatycki, J. (2001). Exposure to titanium dioxide and risk of lung cancer in a population-based study from Montreal. *Scand J Work Environ Health* **27**, 227-232.

Boffetta, P., Soutar, A., Cherrie, J. W., Granath, F., Andersen, A., Anttila, A., Blettner, M., Gaborieau, V., Klug, S. J., Langard, S., Luce, D., Merletti, F., Miller, B., Mirabelli, D., Pukkala, E., Adami, H. O., and Weiderpass, E. (2004). Mortality among workers employed in the titanium dioxide production industry in Europe. *Cancer Causes Control* **15**, 697-706.

Chen, J. L., and Fayerweather, W. E. (1988). Epidemiologic study of workers exposed to titanium dioxide. *J Occup Med* **30**, 937-942.

Cho, W. S., Duffin, R., Poland, C. A., Howie, S. E., MacNee, W., Bradley, M., Megson, I. L., and Donaldson, K. (2010). Metal oxide nanoparticles induce unique inflammatory footprints in the lung: important implications for nanoparticle testing. *Environ Health Perspect* **118**, 1699-1706.

Colvin, V. L. (2003). The potential environmental impact of engineered nanomaterials. *Nat Biotechnol* **21**, 1166-1170.

Craighead, J. E., Abraham, J. L., Churg, A., Green, F. H., Kleinerman, J., Pratt, P. C., Seemayer, T. A., Vallyathan, V., and Weill, H. (1982). The pathology of asbestos-associated diseases of the lungs and pleural cavities: diagnostic criteria and proposed grading schema. Report of the Pneumoconiosis Committee of the College of American Pathologists and the National Institute for Occupational Safety and Health. *Arch Pathol Lab Med* **106**, 544-596.

Donaldson, K., Aitken, R., Tran, L., Stone, V., Duffin, R., Forrest, G., and Alexander, A. (2006). Carbon nanotubes: a review of their properties in relation to pulmonary toxicology and workplace safety. *Toxicol Sci* **92**, 5-22.

Duan, D. M., Wu, N. Q., Slaughter, W. S., Mao, Scott X. (2001). Length scale effect on mechanical behavior due to strain gradient plasticity, *Mat. Sci. Eng. A*, **303** 241-249.

Dreher, K. L. (2004). Health and environmental impact of nanotechnology: toxicological assessment of manufactured nanoparticles. *Toxicol Sci* **77**, 3-5.

El-Chemaly, S., Levine, S. J., and Moss, J. (2008). Lymphatics in lung disease. *Ann N Y Acad Sci* **1131**, 195-202.

El-Chemaly, S., Malide, D., Zudaire, E., Ikeda, Y., Weinberg, B. A., Pacheco-Rodriguez, G., Rosas, I. O., Aparicio, M., Ren, P., MacDonald, S. D., Wu, H. P., Nathan, S. D., Cuttitta, F., McCoy, J. P., Gochuico, B. R., and Moss, J. (2009). Abnormal lymphangiogenesis in idiopathic pulmonary fibrosis with insights into cellular and molecular mechanisms. *Proc Natl Acad Sci U S A* **106**, 3958-3963.

Fryzek, J. P., Chadda, B., Marano, D., White, K., Schweitzer, S., McLaughlin, J. K., and Blot, W. J. (2003). A cohort mortality study among titanium dioxide manufacturing workers in the United States. *J Occup Environ Med* **45**, 400-409.

Hamilton, R. F., Wu, N., Porter, D., Buford, M., Wolfarth, M., and Holian, A. (2009). Particle length-dependent titanium dioxide nanomaterials toxicity and bioactivity. *Part Fibre Toxicol* **6**, 35.

Hardavella, G., Tzortzaki, E. G., Siozopoulou, V., Galanis, P., Vlachaki, E., Avgousti, M., Stefanou, D., and Siafakas, N. M. (2012). Lymphangiogenesis in COPD: Another link in the pathogenesis of the disease. *Respir Med* **106**, 687-693

Harmsen, A. G., Mason, M. J., Muggenburg, B. A., Gillett, N. A., Jarpe, M. A., and Bice, D. E. (1987). Migration of neutrophils from lung to tracheobronchial lymph node. *J Leukoc Biol* **41**, 95-103.

Harmsen, A. G., Muggenburg, B. A., Snipes, M. B., and Bice, D. E. (1985). The role of macrophages in particle translocation from lungs to lymph nodes. *Science* **230**, 1277-1280.

Hayashi, H., and Kobyashi, R. (1996). Daily doses and new technologies about UV protection in patents. *Fragrance Journal* **24**, 53-58.

Holsapple, M. P., Farland, W. H., Landry, T. D., Monteiro-Riviere, N. A., Carter, J. M., Walker, N. J., and Thomas, K. V. (2005). Research strategies for safety evaluation of nanomaterials, part II: toxicological and safety evaluation of nanomaterials, current challenges and data needs. *Toxicol Sci* **88**, 12-17.

Johnson, L. A., and Jackson, D. G. (2008). Cell traffic and the lymphatic endothelium. *Ann N Y Acad Sci* **1131**, 119-133.

Kambouchner, M., and Bernaudin, J. F. (2009). Intralobular pulmonary lymphatic distribution in normal human lung using D2-40 antipodoplanin immunostaining. *J Histochem Cytochem* **57**, 643-648.

Lauweryns, J. M., and Baert, J. H. (1974). The role of the pulmonary lymphatics in the defenses of the distal lung: morphological and experimental studies of the transport mechanisms of intratracheally instillated particles. *Ann N Y Acad Sci* **221**, 244-275.

Leak, L. V. (1980). Lymphatic removal of fluids and particles in the mammalian lung. *Environ Health Perspect* **35**, 55-75.

Li, B., Wang, L. D., Kang, B. N., Wang, P., and Qiu, Y. (2006). Review of recent progress in solid-state dye-sensitized solar cells. *Sol Energ Mat Sol C* **90**, 549-573.

Maynard, A. D., and Kuempel, E. D. (2005). Airborne nanostructured particles and occupational health. *J Nanopart Res* **7**, 587-614.

Mor, G. K., Varghese, O. K., Paulose, M., Shankar, K., and Grimes, C. A. (2006). A review on highly ordered, vertically oriented TiO2 nanotube arrays: Fabrication,

material properties, and solar energy applications. *Sol Energ Mat Sol C* **90**, 2011-2075.

Murphy, F. A., Poland, C. A., Duffin, R., Al-Jamal, K. T., Ali-Boucetta, H., Nunes, A., Byrne, F., Prina-Mello, A., Volkov, Y., Li, S. P., Mather, S. J., Bianco, A., Prato, M., MacNee, W., Wallace, W. A., Kostarelos, K., and Donaldson, K. (2011). Length-Dependent Retention of Carbon Nanotubes in the Pleural Space of Mice Initiates Sustained Inflammation and Progressive Fibrosis on the Parietal Pleura. *Am. J. Pathol.* **178**, 2587-2600.

National Institute for Occupational Safety and Health (2011). Current Intelligence Bulletin 63: Occupational Exposure to Titanium Dioxide. (Department of Health and Human Services, Ed.), pp. 119, Cincinnati, OH.

Nel, A., Xia, T., Madler, L., Lin, N. (2006). Toxic potential of materials at the nanolevel. *Science* **311**, 622–627.

Oberdörster, G., Oberdörster, E., Oberdörster, J. (2005). Nanotoxicology: an emerging discipline evolving from studies of ultrafine particles. *Environ Health Perspect* **113**, 823–39.

Pepper, M. S., and Skobe, M. (2003). Lymphatic endothelium: morphological, molecular and functional properties. *J Cell Biol* **163**, 209-213.

Poland, C. A., Byrne, F., Cho, W. S., Prina-Mello, A., Murphy, F. A., Davies, G. L., Coey, J. M., Gounko, Y., Duffin, R., Volkov, Y., and Donaldson, K. (2011). Length-dependent pathogenic effects of nickel nanowires in the lungs and the peritoneal cavity. *Nanotoxicology* **Epub ahead of print**.

Poland, C. A., Duffin, R., Kinloch, I., Maynard, A., Wallace, W. A. H., Seaton, A., Stone, V., Brown, S., MacNee, W., and Donaldson, K. (2008). Carbon nanotubes

introduced into the abdominal cavity of mice show asbestos-like pathogenicity in a pilot study. *Nat. Nanotechnol.* **3**, 423-428.

Porter, D., Sriram, K., Wolfarth, M., Jefferson, A., Schwegler-Berry, D., Andrew, M., and Castranova, V. (2008). A biocompatible medium for nanoparticle dispersion. *Nanotoxicology* **2**, 144-154.

Porter, D. W., Hubbs, A. F., Mercer, R. R., Wu, N., Wolfarth, M. G., Sriram, K., Leonard, S., Battelli, L., Schwegler-Berry, D., Friend, S., Andrew, M., Chen, B. T., Tsuruoka, S., Endo, M., and Castranova, V. (2010). Mouse pulmonary dose- and time course-responses induced by exposure to multi-walled carbon nanotubes. *Toxicology* **269**, 136-147.

Ramanakumar, A. V., Parent, M. E., Latreille, B., and Siemiatycki, J. (2008). Risk of lung cancer following exposure to carbon black, titanium dioxide and talc: results from two case-control studies in Montreal. *Int J Cancer* **122**, 183-189.

Roggli, V. L., Gibbs, A. R., Attanoos, R., Churg, A., Popper, H., Cagle, P., Corrin, B., Franks, T. J., Galateau-Salle, F., Galvin, J., Hasleton, P. S., Henderson, D. W., and Honma, K. (2010). Pathology of asbestosis- An update of the diagnostic criteria: Report of the asbestosis committee of the college of american pathologists and pulmonary pathology society. *Arch Pathol Lab Med* **134**, 462-480.

Rossi, E. M., Pylkkanen, L., Koivisto, A. J., Vippola, M., Jensen, K. A., Miettinen, M., Sirola, K., Nykasenoja, H., Karisola, P., Stjernvall, T., Vanhala, E., Kiilunen, M., Pasanen, P., Makinen, M., Hameri, K., Joutsensaari, J., Tuomi, T., Jokiniemi, J., Wolff, H., Savolainen, K., Matikainen, S., and Alenius, H. (2010). Airway

exposure to silica-coated TiO2 nanoparticles induces pulmonary neutrophilia in mice. *Toxicol Sci* **113**, 422-433.

Stone, K. C., Mercer, R. R., Gehr, P., Stockstill, B., and Crapo, J. D. (1992). Allometric relationships of cell numbers and size in the mammalian lung. *Am J Respir Cell Mol Biol* **6**, 235-243.

Tafen, D. N., Wang, J., Wu, N., and Lewis, J. P. (2009). Visible light photocatalytic activity in nitrogen-doped TiO(2) nanobelts. *Appl Phys Lett* **94**.

Tan, G. L., Hömmerich, U., Temple, D., Wu, N. Q., Zheng, J. G., Loutts, G. (2003). Synthesis and optical characterization of CdTe nanocrystals prepared by ball milling process, *Scripta Materialia*, **48** 1469-1474.

Takahashi, S., and Patrick, G. (1987). Patterns of lymphatic drainage to individual thoracic and cervical lymph nodes in the rat. *Lab Anim* **21**, 31-34.

Wang, D., Zhao, H., Wu, N., El Khakani, M. A., and Ma, D. (2010). Tuning the Charge-Transfer Property of PbS-Quantum Dot/TiO(2)-Nanobelt Nanohybrids via Quantum Confinement. *J Phys Chem Lett* **1**, 1030-1035.

Wang, J., Manivannan, A., and Wu, N. (2008). Sol-gel derived La(0.6)Sr(0.4)CoO(3) nanoparticles, nanotubes, nanowires and thin films. *Thin Solid Films* **517**, 582-587.

Warheit, D. B., Webb, T. R., Sayes, C. M., Colvin, V. L., and Reed, K. L. (2006). Pulmonary instillation studies with nanoscale TiO2 rods and dots in rats: toxicity is not dependent upon particle size and surface area. *Toxicol Sci* **91**, 227-236.

Watanabe, M., Okada, M., Kudo, Y., Tonori, Y., Niitsuya, M., Sato, T., Aizawa, Y., and Kotani, M. (2002). Differences in the effects of fibrous and particulate titanium

dioxide on alveolar macrophages of Fischer 344 rats. *J Toxicol Environ Health A* **65**, 1047-1060.

Wright, J. L., and Churg, A. (1984). Morphology of small-airway lesions in patients with asbestos exposure. *Hum Pathol* **15**, 68-74.

Wu, N., Wang, J., Tafen, D. N., Wang, H., Zheng, J.-G., Lewis, J. P., Liu, X., Leonard, S. S., and Manivannan, A. (2010). Shape-Enhanced Photocatalytic Activity of Single-Crystalline Anatase TiO(2) (101) Nanobelts. *J Am Chem Soc* **132**, 6679-6685.

Yang, M., Wang, J., Li, H., Zheng, J.-G., and Wu, N. N. (2008). A lactate electrochemical biosensor with a titanate nanotube as direct electron transfer promoter. *Nanotechnology* **19**.

Table 1 Summary of histopathological findings

Post-Exposure (days)	Treatment	Total n	alveolitis	Histiocytic alveolitis	Fibrosis	Phagocytosed Nanoparticles
28	DM	6	0 (n=6)	0 (n=6)	0 (n=6)	0 (n=6)
	7.5 µg NS	5	0 (n=4)	0 (n=5)	0 (n=5)	4 (n=5)*
			2 (n=1)			
	30 µg NS	7	0 (n=7)	0 (n=5)	0 (n=7)	5 (n=7)*
				2 (n=2)		
	7.5 µg NB-1	5	0 (n=4)	0 (n=5)	0 (n=5)	0 (n=3)
			2 (n=1)			2 (n=1)
						4 (n=1)
	30 µg NB-1	6	0 (n=5)	0 (n=2)*	0 (n=5)	4 (n=6)*
			3 (n=1)	3 (n=2)	2 (n=1)	
				4 (n=2)		
	7.5 µg NB-2	6	0 (n=5)	0 (n=5)	0 (n=6)	0 (n=3)
			2 (n=1)	3 (n=1)		4 (n=3)
	30 µg NB-2	7	0 (n=3)*	0 (n=5)	0 (n=4)	0 (n=5)
			3 (n=1)	4 (n=1)	2 (n=1)	4 (n=2)
			4 (n=1)	5 (n=1)	3 (n=2)	
			5 (n=2)			
112	DM	8	0 (n=8)	0 (n=8)	0 (n=8)	0 (n=8)
	7.5 µg NS	9	0 (n=9)	0 (n=9)	0 (n=9)	4 (n=9)*
	30 µg NS	7	0 (n=7)	0 (n=5)	0 (n=7)	4 (n=7)*
				2 (n=2)		
	7.5 µg NB-1	10	0 (n=9)	0 (n=10)	0 (n=9)	0 (n=7)
			4 (n=1)		4 (n=1)	2 (n=2)
						4 (n=1)
	30 µg NB-1	7	0 (n=6)	0 (n=7)	0 (n=5)	0 (n=1)*
			3 (n=1)		2 (n=1)	2 (n=3)
					3 (n=1)	4 (n=3)
	7.5 µg NB-2	8	0 (n=8)	0 (n=7)	0 (n=8)	0 (n=7)
				6 (n=1)		2 (n=1)
	30 µg NB-2	7	0 (n=5)	0 (n=5)	0 (n=3)*	0 (n=4)
			2 (n=1)	2 (n=1)	3 (n=3)	4 (n=3)
			4 (n=1)	3 (n=1)	4 (n=1)	

Values represent histopathology score and inside parentheses the number of animals (n) with that score.
*Significant difference between DM (control) and nanoparticle exposure group.

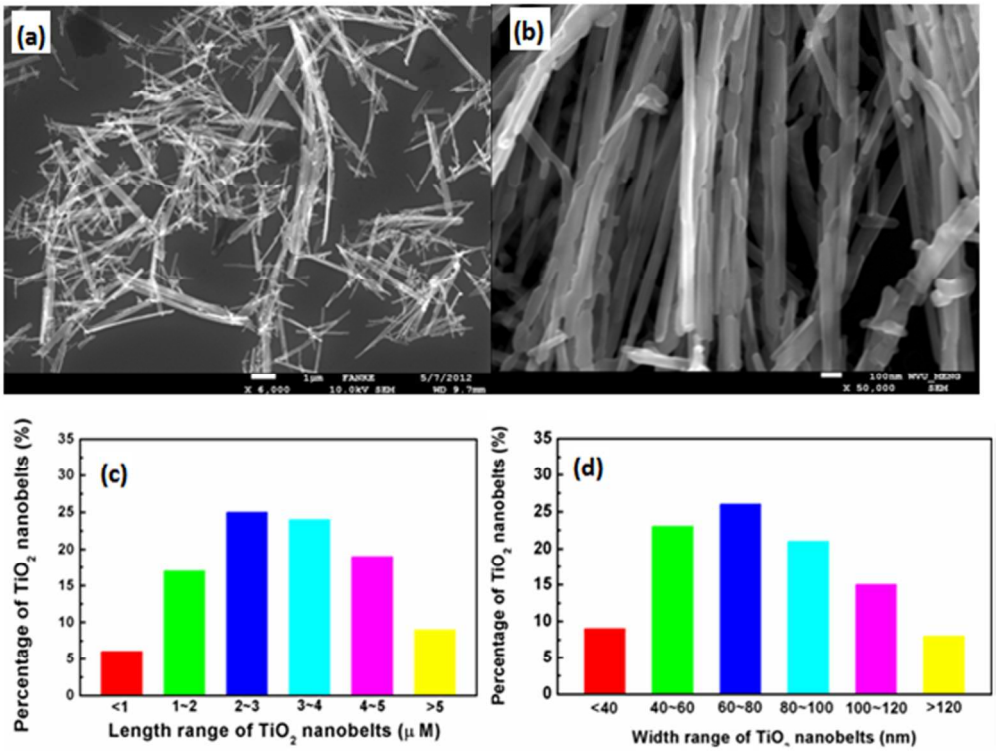

Figure 1. Characterization of nanobelt sample NB1. Panel A. Low-magnification SEM image of nanobelt sample NB1. Panel B. High-magnification SEM image of nanobelt sample NB1. Panel C. Histogram of lengths of nanobelt sample NB1. Panel C. Histogram of widths of nanobelt sample NB1.
177x134mm (300 x 300 DPI)

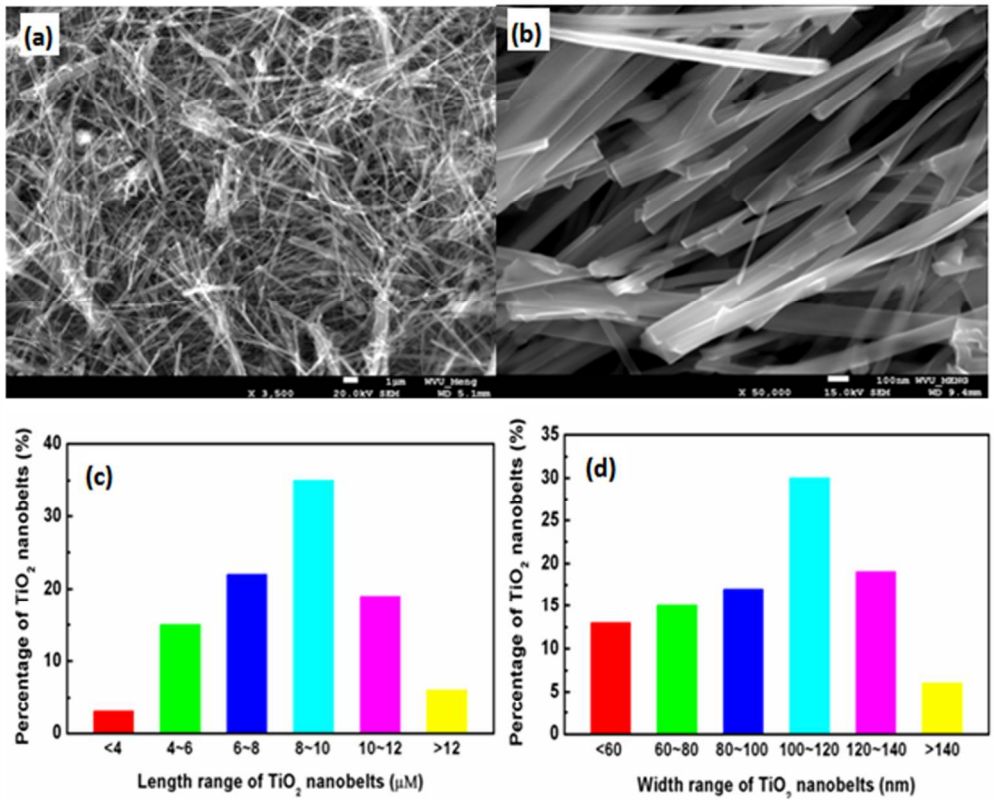

Figure 2. Characterization of nanobelt sample NB2. Panel A. Low-magnification SEM image of nanobelt sample NB2. Panel B. High-magnification SEM image of nanobelt sample NB2. Panel C. Histogram of lengths for nanobelt sample NB2. Panel D. Histogram of widths for nanobelt sample NB2.
177x142mm (300 x 300 DPI)

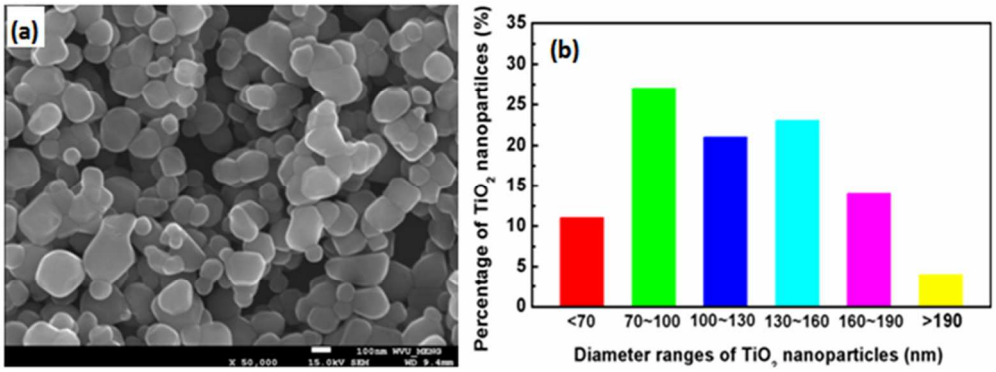

Figure 3. Characterization of nanosphere sample NS. Panel A. SEM image of nanosphere sample NS. Panel B. Size distribution for nanosphere sample NS.
177x67mm (300 x 300 DPI)

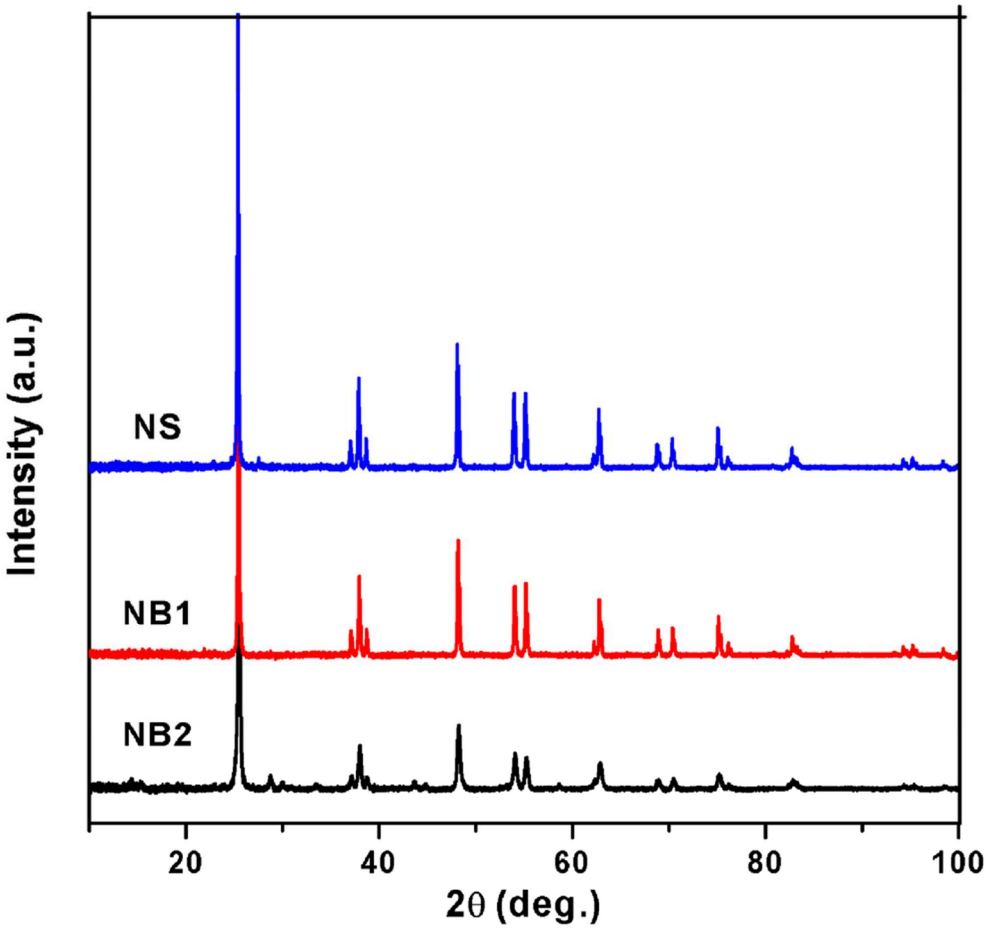

Figure 4. XRD patterns for nanospheres (NS), short (NB1) and long (NB2) nanobelt samples.
84x80mm (300 x 300 DPI)

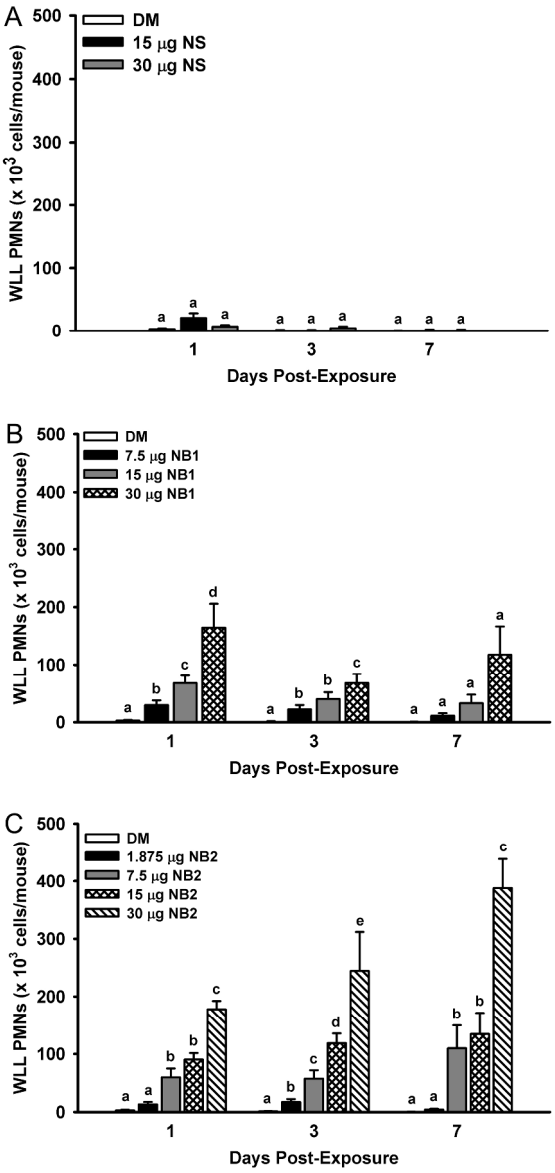

Figure 5. Acute pulmonary inflammation dose-responses after exposure to TiO_2 nanoparticles. WLL PMNs were determined at 1, 3 and 7 days post-exposure as an indicator of pulmonary inflammation. Panel A. WLL PMNs determined after exposure to NS. Panel B. WLL PMNs determined after exposure to NB1. Panel C. WLL PMNs determined after exposure to NB2. Values represent means ± SE (n=6-8). For a given post-exposure time, bars with different letters are significantly different from each other ($p<0.05$).

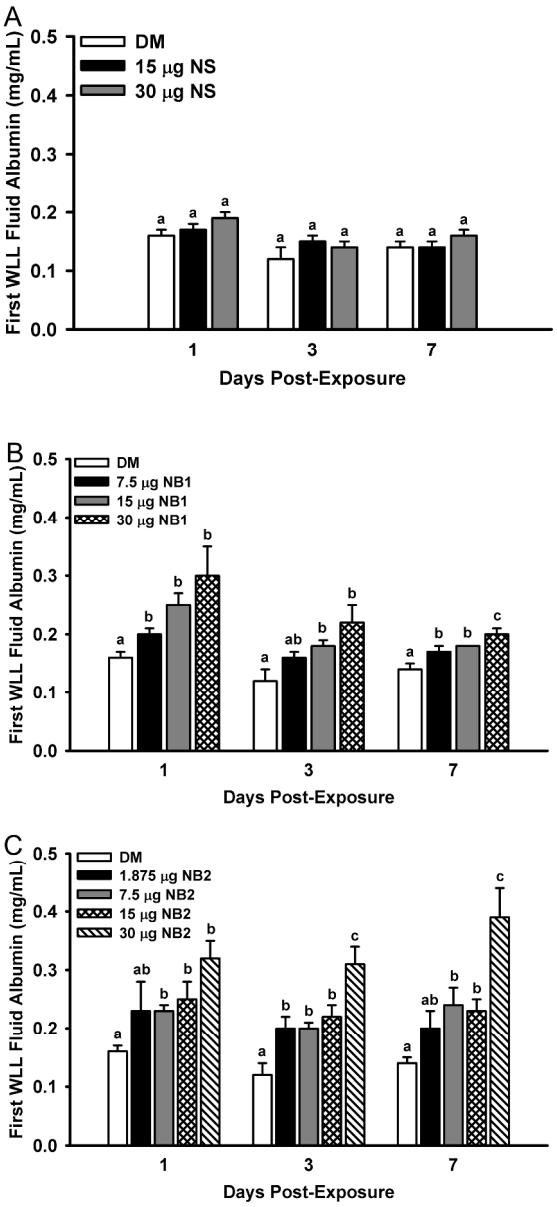

Figure 6. Acute pulmonary first WLL fluid albumin dose-responses after exposure to TiO_2 nanoparticles. First WLL fluid albumin concentrations were determined at 1, 3 and 7 days post-exposure as an indicator of the integrity of the lung blood-gas barrier. Panel A. First WLL fluid albumin concentrations determined after exposure to NS. Panel B. First WLL fluid albumin concentrations determined after exposure to NB1. Panel C. First WLL fluid albumin concentrations determined after exposure to NB2. Values represent means ± SE (n=6-8). For a given post-exposure time, bars with different letters are significantly different from each other ($p<0.05$). Bars with two letters indicate differences exist between this bar and both lower and/or higher doses at the same post-exposure time.

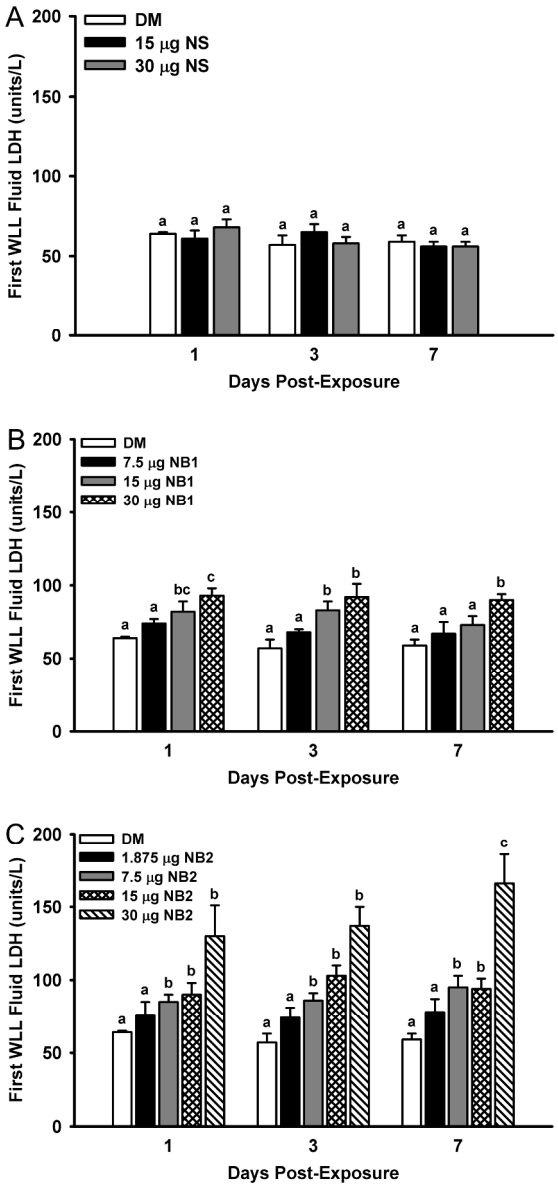

Figure 7. Acute pulmonary first WLL fluid LDH dose-responses after exposure to TiO_2 nanoparticles. First WLL fluid LDH was determined at 1, 3 and 7 days post-exposure as an indicator of the cytotoxicity. Panel A. First WLL fluid LDH activities determined after exposure to NS. Panel B. First WLL fluid LDH activities determined after exposure to NB1. Panel C. First WLL fluid LDH activities determined after exposure to NB2. Values represent means ± SE (n=6-8). For a given post-exposure time, bars with different letters are significantly different ($p<0.05$). Bars with two letters indicate differences exist between this bar and both lower and/or higher doses at the same post-exposure time.

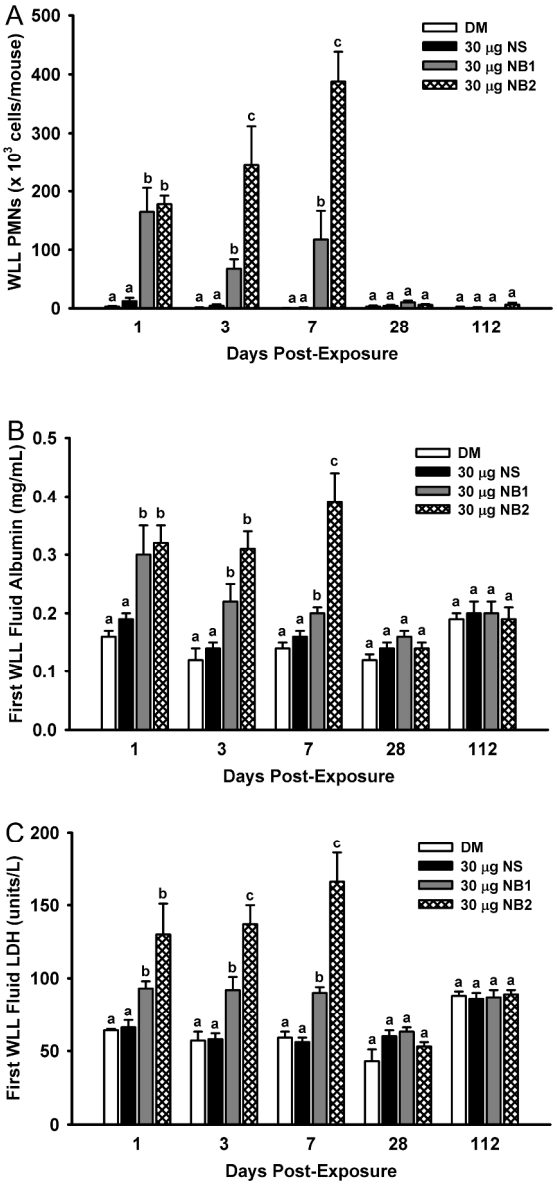

Figure 8. Time course of pulmonary inflammation and damage after exposure to TiO_2 nanoparticles. Panel A. WLL PMNs were determined as an indicator of pulmonary inflammation. Panel B. First WLL fluid albumin concentrations were determined as an indicator of the integrity of the lung blood-gas barrier. Panel C. First WLL fluid LDH was determined as an indicator of nanoparticle-induced cytotoxicity. Values represent means ± SE (n=6-8). For a given post-exposure time, bars with different letters are significantly different from each other ($p<0.05$).

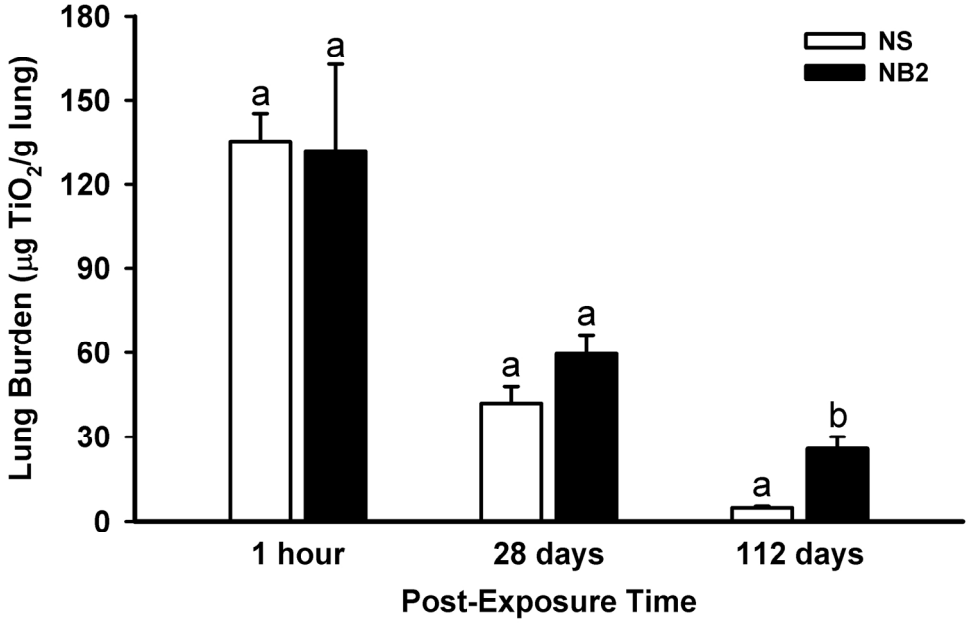

Figure 9. TiO_2 nanoparticle lung burden. The lung burden of TiO_2 NS and NB2 were determined from 1 hour to 112 days post-exposure. Values represent means ± SE (n=5). For a given post-exposure time, bars with different letters are significantly different ($p<0.05$).

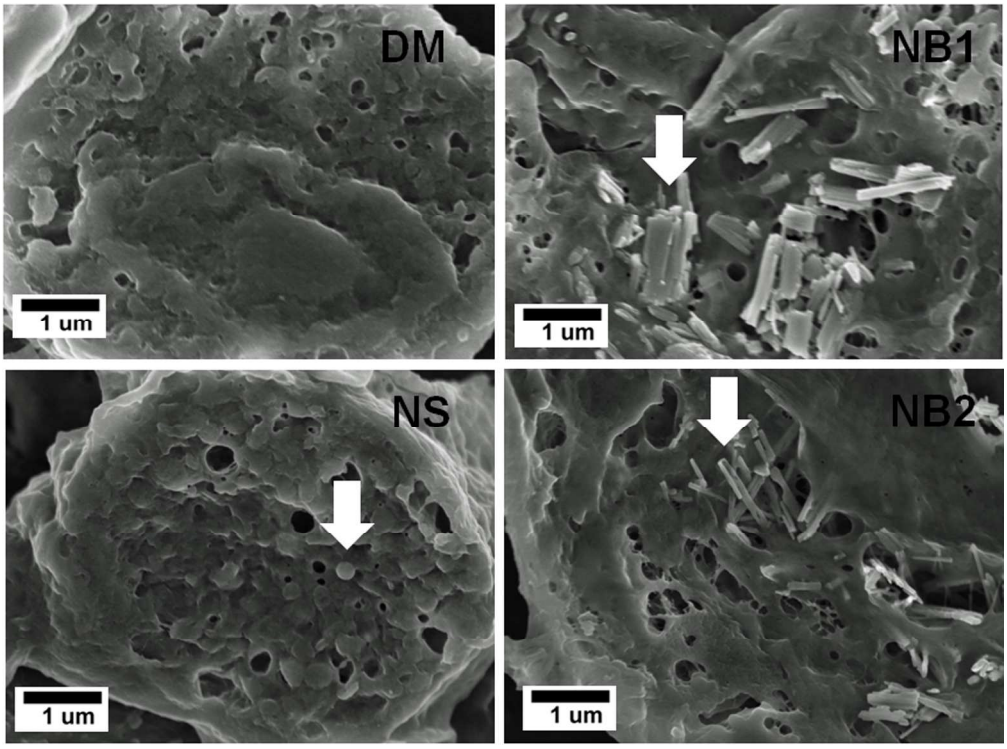

Figure 10. Field emission scanning electron microscope (FESEM) showing interior view of AMs isolated from mice exposed to DM, NS (30 μg), NB1 (30 μg) or NB2 (30 μg) at 112 days post-exposure. Arrows indicate nanoparticles within AMs.

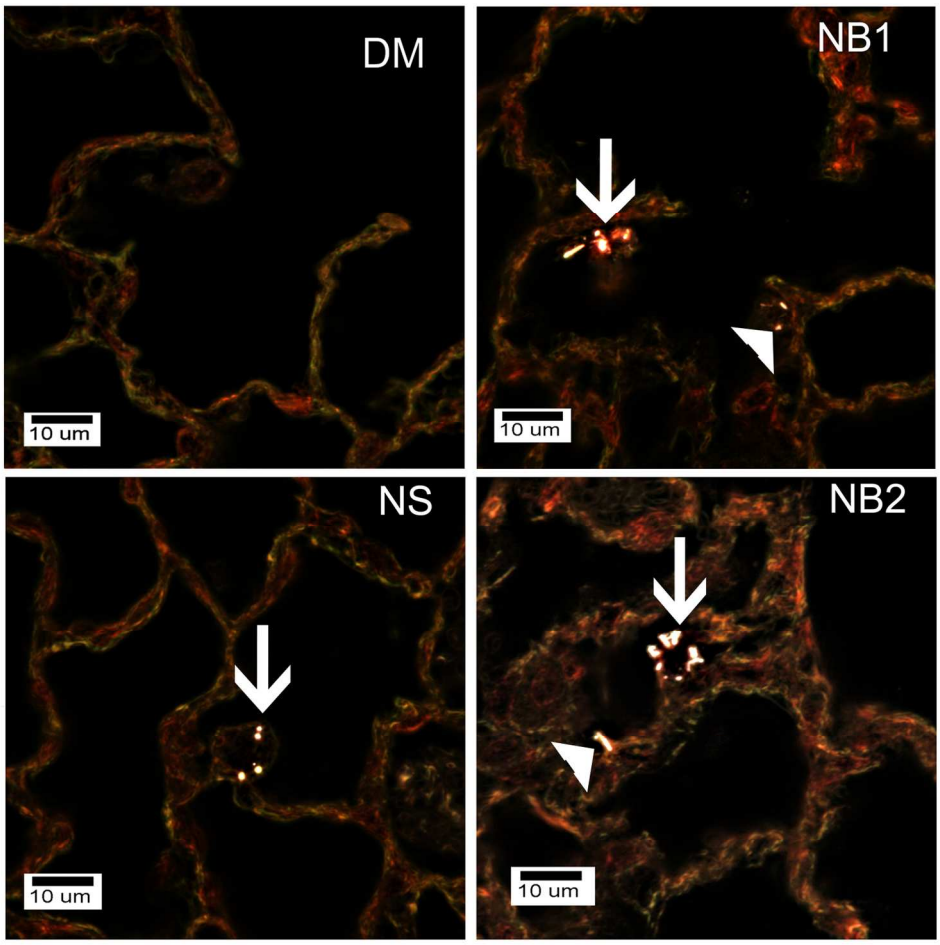

Figure 11. Enhanced dark field microscopy examination of mice exposed to DM, NS (30 µg), NB1 (30 µg) or NB2 (30 µg) at 112 days post-exposure. Nanospheres and nanobelts are generally white against the dull colored background of tissue in these images. Arrows in the figure indicate alveolar macrophages which contain NS, NB1 or NB2 in the respective figures. Filled triangles indicate nanobelts which are either contained in or penetrating into the alveolar interstitial space. NS were infrequently observed in the lungs as the total lung burden remaining at 112 days post-exposure was less than 4% of initial lung burden. No nanoparticles were observed in lungs from DM-exposed mice.
177x167mm (300 x 300 DPI)

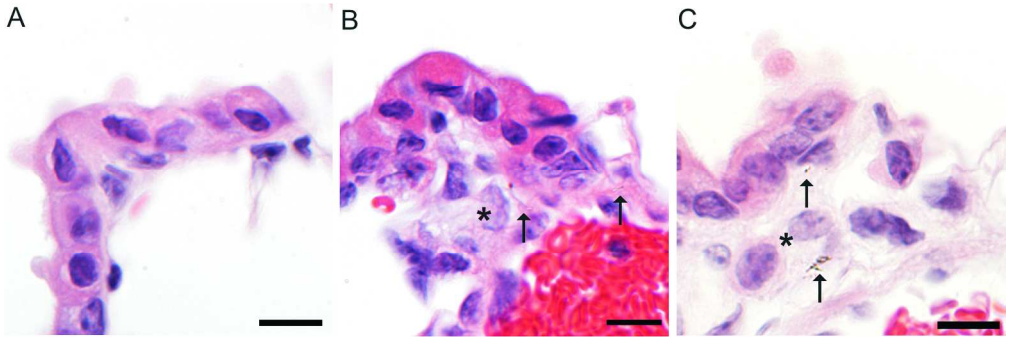

Figure 12. Bronchioloalveolar junction at 112 days post-exposure to 30 μg TiO_2 nanoparticles. Panel A. Normal bronchioloalveolar junction in a NS-exposed mouse. Panel B. Rare NB1 (arrows) and small numbers of infiltrating histiocytes (*) in a NB1-exposed mouse. Panel C. Rare NB2 (arrows) and small numbers of infiltrating histiocytes (*) in a NB1-exposed mouse. Reference bar is 10 microns.

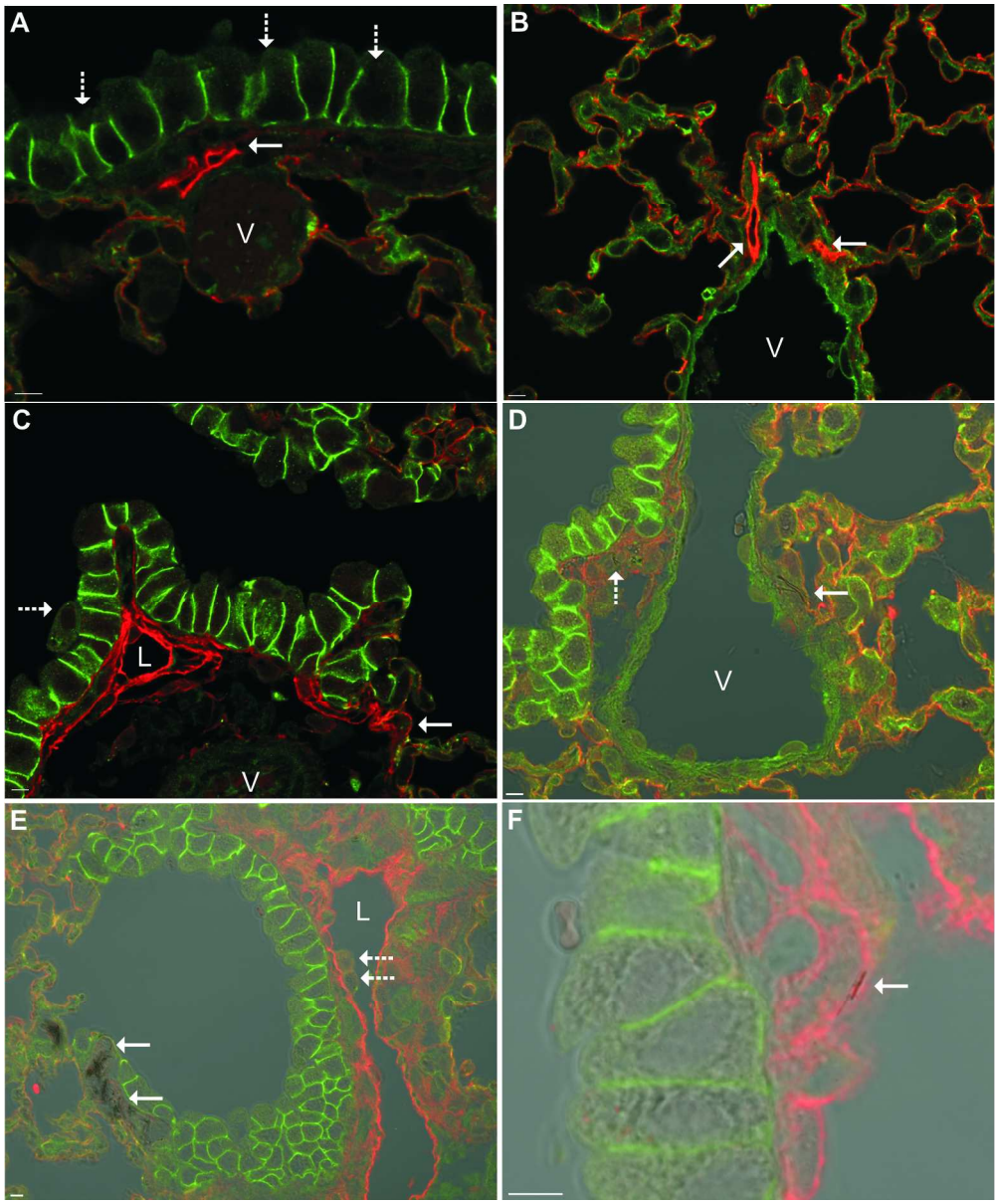

Figure 13. Podoplanin/e-cadherin dual-label immunofluorescence at 112 days post-exposure to 30 μg of a TiO_2 nanoparticle. Podoplanin (red) is expressed in lymphatic endothelium and alveolar type I cells. E-cadherin (green) is expressed in the intercellular junction of airway epithelial cells and lightly stains alveolar type I cells. In the combined images, the lymphatic endothelium is bright red, alveolar type I cells are orange, intercellular junctions of airway epithelial cells are bright green and the vascular endothelium is pale green. Panel A. In a mouse exposed to NS, peribronchiolar lymphatics (solid arrow) are small structures subjacent to the bronchiolar epithelium (dashed arrows) and are easily distinguished from the vasculature (V). Panel B. In a mouse exposed to NS, perivascular lymphatics (solid arrows) are in the tunica adventitia of large vessels (V). Panel C. In a mouse exposed to NB1, the smallest lymphatic capillaries are located near the bronchioloalveolar junction (solid arrow), the peribronchiolar lymphatics are unusually prominent and occasionally dilated (L) but easily distinguished from the vasculature (V). A macrophage (dashed) arrow is being cleared by mucociliary clearance. Panel D. In a mouse exposed to NB1, transmitted light is being used to visualize aggregates of NB1 nanobelts in sites where the lymphatics are frequently located: NB1 (solid

arrow) are in the tunica adventitia of a large vessel (V) and in the peribronchiolar interstitium (dashed arrow). Panel E. In a mouse exposed to NB2, transmitted light is being used to visualize aggregates of NB2 nanobelts (solid arrows) in the interstitium subjacent to the epithelium at the bronchioloalveolar junction. A peribronchiolar lymphatic (L) is markedly dilated and macrophages (dashed arrow) are adhered to the lymphatic endothelium. Panel F. Refocusing and a higher magnification of the section in Panel E reveals a NB2 (solid arrow) in the lymphatic endothelium. Reference bar is 5 microns.